Applied Catalysis B: Environmental 206 (2017) 89–103

Contents lists available at ScienceDirect

Applied Catalysis B: Environmental

journal homepage: www.elsevier.com/locate/apcatb

Review

Visible-to-ultraviolet Upconvertion: Energy transfer, material matrix, and synthesis strategies

Wenyan Zhang[a,b,c], Songlin Yang[d], Jian Li[d], Wei Gao[a,b], Yibing Deng[d], Wenping Dong[d], Chengjian Zhao[d], Gongxuan Lu[a,*]

[a] State Key Laboratory for Oxo Synthesis and Selective Oxidation, Lanzhou Institute of Chemical Physics, Chinese Academy of Science, Lanzhou 730000, China
[b] University of Chinese Academy of Science, Beijing 10080, China
[c] College of Material Engineering, Jinling Institute of Technology, Nanjing, China
[d] China Astronaut Research and Training Center, Beijing, 100094, China

ARTICLE INFO

Article history:
Received 30 November 2016
Received in revised form
30 December 2016
Accepted 8 January 2017
Available online 10 January 2017

Keywords:
Upconversion (UC)
Material
Visible-to-UV
Synthesis techniques
Photo-reactions
Photocatalysis

ABSTRACT

In recent years, Upconversion (UC) material has attracted much attention because of its fantastic energy transfer capability of converting the low-energy photons into high-energy photons via anti-Stokes process. Among UC materials, the visible-to-UV UC materials exhibit remarkable potential in laser conversion, photo-catalysis, the sterilization as well as antibiosis in biological areas because of their capability of converting the visible radiation into ultraviolet emission. Considering the interesting UC process and large potential application of the visible-to-UV UC materials, it is necessary to overview its intrinsic UC mechanism, material structure, as well as material synthesis techniques for the development of UC material. This work focus on the visible-to-UV UC materials and review its current research situation, the challenges in its research field, as well as analyzing and comparing recent investigations to provide valuable evaluation for such materials both from theoretical and commercial perspective. The most effective UC matrix and luminescent centers in recent works were summarized and the intrinsic mechanisms of visible-to-UV UC were introduced. The material design strategies and techniques for the synthesis of visible-to-UV UC phosphors were focused. The advantages and the limitations of visible-to-UV UC material are discussed in detail, and a reasonable expectation for the emerging trends of such potential material is provided.

© 2017 Elsevier B.V. All rights reserved.

Contents

1. Introduction 90
2. Visible-to-UV UC mechanism 91
   2.1. UC mechanism of the lanthanide-doped inorganic phosphors 91
      2.1.1. UC process in visible-to-UV energy transfer 91
      2.1.2. Electron energy level of Pr^{3+} ion and its important role in visible-to-UV energy transfer 91
   2.2. Organic sensitizer/acceptor systems 92
3. Material matrices 93
   3.1. UC mechanism of the lanthanide-doped inorganic phosphors 93
      3.1.1. The fluoride matrices 93
      3.1.2. The silicates matrices 94
   3.2. Organic sensitizer/acceptor systems 96
4. Characteristic strategies for the visible-to-UV UC material 96
   4.1. Optical characterization strategies 97
   4.2. Crystal structure characterization 97

* Corresponding author.
E-mail address: gxlu@lzb.ac.cn (G. Lu).

http://dx.doi.org/10.1016/j.apcatb.2017.01.023
0926-3373/© 2017 Elsevier B.V. All rights reserved.

4.2.1. Powder XRD 98
4.2.2. X-ray absorption spectrum (XAS) 98
4.2.3. HRTEM and STEM 98
4.3. Size and morphology characterization 98
4.4. Composition and elements concentration characterization 99
4.4.1. EDS, EELS and XPS characterization 99
4.4.2. ICP-MS and ICP-AES characterization 99
5. Synthesis technique for the visible-to-UV UC material 99
5.1. Solid state reaction 99
5.2. Sol-gel technique 100
5.3. Hydrothermal synthesis technique 100
6. Challenges in visible-to-UV UC material research field 100
6.1. Challenges for lanthanide-doped inorganic phosphors 100
6.2. Challenges for organic sensitizer/acceptor systems 100
7. Perspective and potential applications of the visible-to-UV UC material 100
7.1. Perspective of lanthanide-doped inorganic phosphors 100
7.1.1. Potential in the biomaterial fields 100
7.1.2. Potential in photocatalysis 101
7.2. Perspective of organic sensitizer/acceptor systems 102
Notes 102
Acknowledgments 102
References 102

1. Introduction

In recent years, Upconversion (UC) material has attracted much attention because of its fantastic energy transfer capability of converting the low-energy photons into high-energy photons via anti-Stokes process [1–7]. During the anti-Stokes process, two or more photons were absorbed sequentially by a material to reach an excited state, which could then release one higher-energy photon. According to the wavelength range of energy transfer, current research of UC materials could be classified into three types: (1) the IR-to-visible UC materials which could transfer infrared (IR) light to visible light due to their NIR-triggered anti-Stokes emissions, (2) the visible-to-UV UC materials which could transfer visible light to ultraviolet (UV) light, and (3) the visible-to-visible UC materials which could transfer long-wavelength visible light to short-wavelength light [6]. Table 1 summarized the advantages and disadvantages of those UC materials in terms of their anti-Stokes shifts, chemical stability, UC conversion efficiency, toxicity, synthesis cost and mechanical stability. Application potential of the three materials not only depends on their UC capability, but is closely related to their chemical stability, toxicity, and synthesis cost.

Owing to their unique chemical and physical advantages (Table 1), the IR-to-visible UC materials exhibit wide potential in the fields of photocatalysis, optoelectronic devices, displays, solar cells, nonlinear optics, bio-imaging and molecular probes [8–14]. There are enormous progresses in the developments of IR-to-visible UC materials since the birth of the $NaYF_4$:Er^{3+},Yb^{3+} system in 1966 [10,11,13,14]. Current research situation not only focus on exploring appropriate luminescent centers and sensitizer, but construct high efficient material matrix for UC energy transfer. Various IR-to-visible UC materials have been invented, such as the Gd_2O_3:Yb^{3+}/Tm^{3+} nanoparticles, Er^{3+}/Tm^{3+}/Yb^{3+} tridoped ($NaY(WO_4)_2$/YF_3), and β-$NaYF_4$:Yb^{3+}/Er^{3+}. Those works indicate that hexagonal $NaYF_4$ is the most efficient matrix for IR-to-visible UC generation. Meanwhile, current research recognized that Yb^{3+} is the most effective sensitizer in IR-to-visible UC materials, owing to its simple 4f electronic structure and ability to enhance absorption and energy transfer without inducing quenching of excited activator ions [8,10,13,14]. A key challenge in IR-to-visible UC research fields is the UC efficiency are reduced due to large amounts of defects and dangling bonds on the surface of UC phosphors. This challenge triggered current boom of constructing core-shell and core-shell-shell sandwich structure research to down lower energy transfer loss and endow the IR-to-visible UC materials with novel optical/electronic properties.

Visible-to-UV UC materials facilitate the visible to UVC (220–280 nm) energy transfer via visible-light-triggered anti-Stokes emissions [18]. Research situation of visible-to-UV UC materials lags far behind that of IR-to-visible UC materials. The development of visible-to-UV UC materials mainly endure two challenges: one is lacking appropriate luminescent centers which have energy level to facilitate the visible-to-UV UC transition, the other is lacking of suitable material matrices which contain low phonon energy, high tolerance, and favorable chemical stability to provide the luminescent centers with an efficient energy transfer environment [15–18]. Nevertheless, considering that more than 50% of the solar spectrum is in the range of visible light, it could be expected that the visible-to-UV UC material will show remarkable potential in exploring solar energy to resolve present energy crisis and severe environmental problems of the world by taking advantage of stable semiconductor photocatalysts sensitive to UV light in water splitting to hydrogen. For instance, current research of visible-light-driven water splitting is highly limited due to absence of efficient and chemically stable photo-catalysts. TiO_2 and Ti based photocatalysts mainly respond to UV irradiation, so they could not make full use of the whole solar spectrum. Sulfide and Selenide based photo-catalysts could work under visible light irradiation, but their practical applications are highly restricted due to their poor photo-chemical stability (photocorrosion). The application of visible-to-UV UC material can effectively sensitize UV-responsive photocatalysts to promote visible-light driven water splitting. Besides, in biological research fields, visible-to-UV UC material also show huge potential that they exhibited amazing effects on sterilization and antibiosis even when the Visible-to-UV UC conversion efficiency is lower than 0.1%. Consequently, the Visible-to-UC UC materials could open a new window for making full use of sustainable solar energy.

Driven by great application potential of visible-to-UV UC material in energetic, environmental and biological research fields, it is necessary to summarize the mechanisms, matrix types, material design and synthesis techniques in detail for the development of such important material. In this review, it begins by summarizing the intrinsic mechanisms reported for visible-to-UV UC. Then, the most effective matrix types and luminescent centers in recent

Table 1
Advantages (+) and Disadvantages (−) of different classes of the UC materials.

IR-to-visible UC Material (Ln^{3+}-Doped phosphors)	Visible-to-UV UC Material (Ln^{3+}-Doped phosphors)	Visible-to-visible UC (Organic TTA system)
(+)large anti-Stokes shifts	(+)large anti-Stokes shifts	(−)small anti-Stokes shifts
(−)Poor conversion at low powers	(−)Poor conversion at low powers	(+)Higher conversion at low powers
(−)Narrow absorption bands	(−)Narrow absorption bands	(+)broad absorption bands
(+)Relatively high UC conversion efficiency	(−)Relatively low UC conversion efficiency	(+)Relatively high UC conversion efficiency
(+)High Chemical stability (resisting oxygen/photo damage)	(+)High Chemical stability (resisting oxygen/photo damage)	(−)Low chemical stability (susceptible to oxygen/photo damage)
(+)Low- toxicity	(+)Low- toxicity	(−)High toxicity
(+)Low cost	(+)Low cost	(−)Relatively high cost
(+)Mechanical stability	(+)Mechanical stability	(−)Low mechanical stability

researches were introduced. In addition, this review summarized the material design as well as modern techniques for the synthesis of visible-to-UV UC phosphors. Based on above summarization and analysis, we discuss in detail about the advantages and the limitations of visible-to-UV UC material, and provided a reasonable expectation for the emerging trends of such potential material.

2. Visible-to-UV UC mechanism

2.1. UC mechanism of the lanthanide-doped inorganic phosphors

Up conversion (UC) materials are capable of capturing two or lower energy photons via intermediate excited states, and then emit one higher energy photon to realize the up-conversion for low energy photos. Generally speaking, the UC materials which reported thus far could be divided into two classes: (1) lanthanide-doped inorganic phosphors and (2) organic sensitizer/acceptor systems. The two kinds of visible-UV UC material have different energy transfer capability, energy conversion range and different up-conversion mechanisms. Lanthanide-doped inorganic phosphors could convert visible light to UVA, UVB and UVC (visible-to-UVA/UVB/UVC), whereas the organic sensitizer/acceptor systems could convert visible light to UVA (visible-to-UVA).

2.1.1. UC process in visible-to-UV energy transfer

The lanthanide-doped inorganic phosphors are constructed by embedding the luminescent lanthanide (Ln^{3+}) ions into the inorganic matrix to replace some cations in the matrix. The UC mechanism of lanthanide-doped inorganic phosphors is closely related to the partially filled 4f sub-shells of the Ln^{3+} ions, as the UC energy transfers are generated intrinsically among the abundant intermediate energy levels of those 4f sub-shells [1,4,19]. As illustrated in Fig. 1, the UC mechanisms could be categorized into five classes: (a) excited state absorption (ESA, Fig. 1(a)), (b) energy transfer UC (ETU, Fig. 1(b)), (c) photon avalanche (PA, Fig. 1(c)), (d) cooperative energy transfer (CET, Fig. 1(d)), and (e) energy migration-mediated UC (EMU, Fig. 1(e)) [4]. It is worth noting that different energy transfer processes result in distinct UC efficiencies, and that there is no universal mechanism for any of the luminescent Ln^{3+} ions. Owing to those UC processes, multiple photons could be captured, transferred to excited energy levels, and then relaxed to ground state via radiative transition to emit UC fluorescence.

The IR-to-visible UC could be attributed to one or several of above five mechanisms. However, only the ESA and ETU mechanism have been reported attributing to the UC visible-to-UV energy transfer. In the case of ESA, a single ion was pumped to its excited intermediate state after successively absorbing the energy of two photons, and UC fluorescence was released when the excited electron transferred back to the ground state via radiation relaxation. In terms of the ETU process, it is known that energy transfer occurs between two neighboring ions (one as the sensitizer and the other as the activator) rather than successively absorption of two photons in a single ion. Thus, both ETU UC and the lifetime of electrons at intermediate excited state are highly influenced by the distance between neighboring ions.

According to the process of ESA and ETU, the quantum efficiency of Visible-to-UV UC depend on four factors: (1) whether the Ln^{3+} ions has suitable 4f sub-shells to generate UC; (2) whether the Ln^{3+} ions has long-lifetime intermediate state for excited electrons to stay at; (3) whether the inorganic material matrix could transfer the excitation energy effectively to the Ln^{3+} ions to promote the ESA and ETU; (4) the concentration and distribution of the Ln^{3+} ions in the matrix, taking into account that the energy could not be transferred effectively between two Ln^{3+} ions if the distances between them are too large whereas the aggregation of Ln^{3+} ions will result in fluorescence quenching.

2.1.2. Electron energy level of Pr^{3+} ion and its important role in visible-to-UV energy transfer

Pr^{3+} ion is considered to be the most effective Ln^{3+} ion to generate the visible-to-UV UC, as the electron distribution in its $4f^n$ discrete energy levels could facilitate the excited-state absorption (ESA) and energy transfer upconversion (ETU) for visible irradiation [17]. The ESA process includes two consecutive excitation steps on a single Pr^{3+} ion, such as the process $^3H_4 \rightarrow {}^3P_0 \rightarrow$ 4f5d, as indicated in Fig. 2 [17,20]. In ETU process, two Pr^{3+} ions at $^3P_0$ state interact with each other. In other words, one Pr^{3+} transfer its energy to the other one, so one Pr^{3+} goes back to the $^3H_4$ ground state, while the other one was excited into the 4f5d band. In addition, some research reported a special ESA process which involves a $^3P_J \rightarrow {}^1D_2$ relaxation, as shown in Fig. 3 [16,21]. As the 488 nm light energy coincides with the $^3H_4 \rightarrow {}^3P_0$ transition energy of Pr^{3+} ion, exciting the Pr^{3+} ion by 488 nm irradiation could facilitate both ESA and ETU transition, thus effectively promote the visible-to-UV UC quantum efficiency of Pr^{3+} to emit visible-to-UV UC fluorescence (260–350 nm) under the 488 nm excitation.

Except for the 488 nm irradiation, the visible-to-UV UC could also be excited by 445–455 nm and 470–490 nm irradiations due to the absorption wave-lengths of the $^3P_2$, $^1I_6$, $^3P_1$, and $^3P_0$ intermediate energy levels. Furthermore, it was reported that the visible-to-UV UC of Pr^{3+} ion could be generated by the irradiation of multi-wavelengths [22]. As illustrated in Fig. 4, the visible-to-UV UC of Pr^{3+} could be excited by multi-colored laser beam which combined the violet (447 nm) and green (515 nm) irradiation [22]. As the 447 nm and 515 nm irradiation respectively coincide with the $^3P_0 \rightarrow$ 4f5d and $^3H_4 \rightarrow {}^1D_2$ energy transition of Pr^{3+}, the cooperation of the two irradiation could facilitate the ESA process for the visible-to-UV UC of Pr^{3+}. In addition, the ESA process of Pr^{3+} could also be excited by the multi-colored laser which combined the violet (447 nm) and yellow (589 nm) irradiation, considering that the 447 nm and 589 nm irradiation respectively coincide with the $^1D_2 \rightarrow$ 4f5d and $^3H_4 \rightarrow {}^1D_2$ energy. In consequence, the Pr^{3+}-

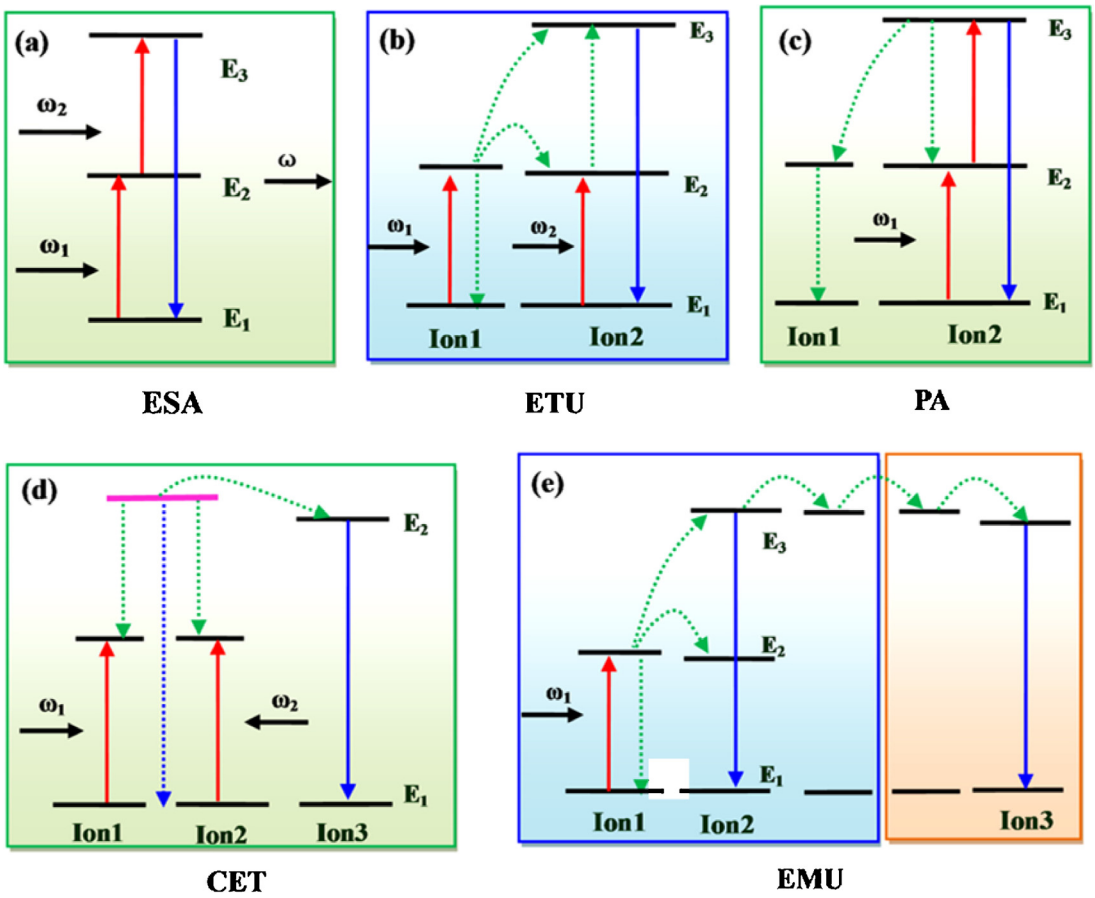

Fig. 1. Figure of the UC processes (a) ESA, (b) ETU, (c) PA, (d) CET, (e) EMU. (red arrow: direct excitation; blue arrows: radiative emission; Dashed green arrow: energy transfer; Different kinds of luminescent centers are shown with different colored energy levels, and different regions are highlighted with different background colors.). (For interpretation of the references to colour in this figure legend, the reader is referred to the web version of this article.)

doped inorganic phosphors have potential to harvest the energy of full solar spectrum for the generating of visible-to-UV UC.

2.2. Organic sensitizer/acceptor systems

In the organic sensitizer/acceptor systems, triplet sensitizer and acceptor are applied to generate the UC conversion via the triplet–triplet annihilation mechanism (TTA). As illustrated in Fig. 5, the TTA mechanism are composed of four important processes as follows[6,2]: (1) a ground-state sensitizer molecule ($^1SENS^0$) harvest the excitation energy and was excited to its singlet state ($^1SENS^*$); (2) the singlet state sensitizer ($^1SENS^*$) relaxed to its triplet state ($^3SENS^*$) via intersystem crossing; (3) the energy of a triplet state sensitizer ($^3SENS^*$) was transferred to a triplet acceptor molecule ($^3ACC^*$) via triplet–triplet energy transfer; (4) two triplet state acceptors ($^3ACC^*$) annihilated to produce an excited singlet photon with high energy ($^1ACC^*$); (5) the UC fluorescence were emitted when the excited singlet photon of acceptor ($^1ACC^*$) transfer back to its ground state ($^1ACC^0$) via spin-allowed radiation relaxation.

According to the TTA mechanism, the energy matching of sensitizer and acceptor is essential for the generation and UC quantum efficiency improvement of the organic sensitizer/acceptor systems. Besides, such TTA UC mechanism endowed the organic sensitizer/acceptor systems with several advantages, including tunable excitation/emission wavelength as well as low excitation energy. On one hand, it is very convenient to regulate the excitation/emission wavelength in such systems by independently selecting appropriate triplet sensitizers/acceptors. On the other

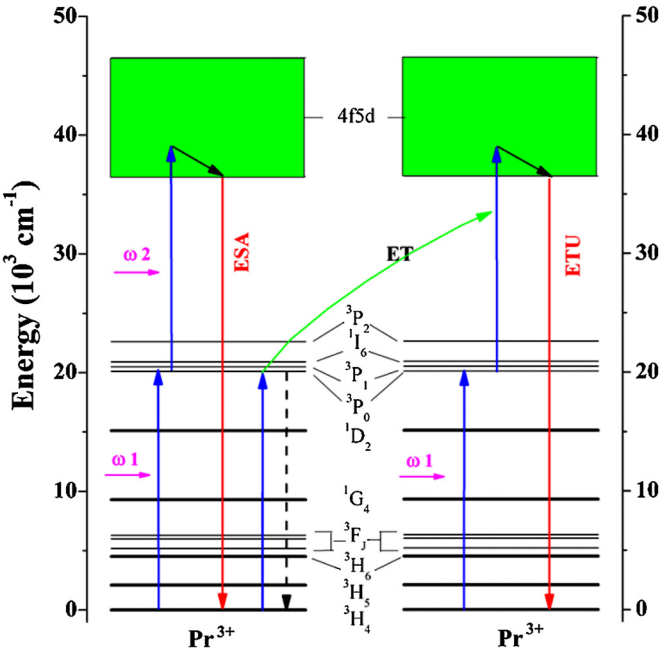

Fig. 2. The excited-state absorption (ESA) and energy transfer upconversion (ETU) of Pr^{3+} ion.

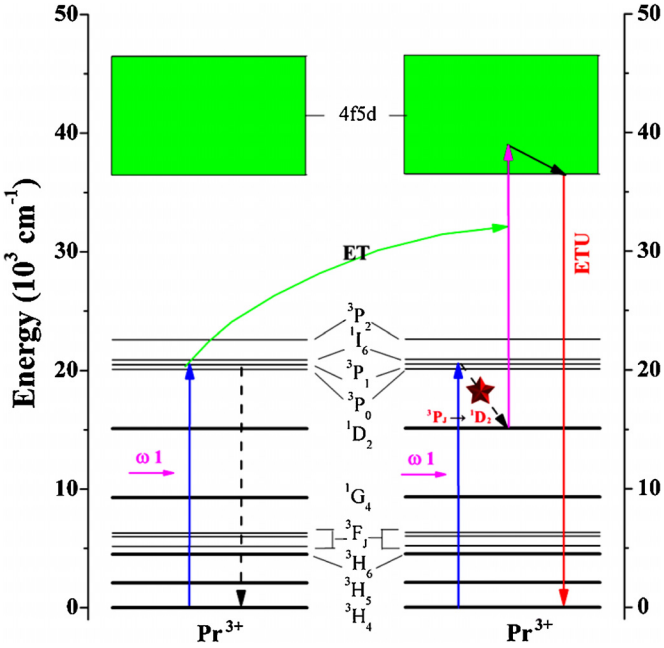

Fig. 3. The energy transfer upconversion (ETU) of Pr^{3+} ion (with $^3P_J \rightarrow {}^1D_2$ relaxation).

hand, the UC fluorescence could be generated by low excitation energy when utilizing the sensitizer which could be excited by low irradiation. So the organic sensitizer/acceptor systems could effectively harvest the whole spectral range of solar light.

3. Material matrices

3.1. UC mechanism of the lanthanide-doped inorganic phosphors

The lanthanide-doped inorganic phosphors are composed of inorganic matrices and Ln^{3+} ions which replaced some sites of the matrices. According to the ESA and ETU mechanisms, the visible-to-UV UC quantum efficiency not only relies on the electron level, concentration and distribution of the Ln^{3+} ions, but on the composition, crystal structure and energy transfer capability of the host matrix. In order to provide an effective energy transfer environment for the Ln^{3+} ions to produce Visible-to-UV UC, an ideal host matrix should be equipped with four characteristics: (a) high tolerance for the doping of Ln^{3+} ions, (b) low phonon energy to minimize the non-radiative relaxations, (c) high transparency for the visible photons to migrate freely, (d) favorable chemical and thermal stabilities.

Until now, only a few kinds of inorganic matrices have been reported to have the visible-to-UV UC capability. According to their composition, those inorganic matrices could be classified to be fluoride, silicates and aluminates [15–18,20–26]. In this review, we mainly focused on discussing and summarizing the fluoride and silicates matrix, as the two types of matrix have higher visible-to-UV UC efficiency than others. Those inorganic matrices could also be classified to be micro/nano-crystals and ceramics, according to their morphology and size. In this review, the material matrixes are summarized and investigated in terms of their composition classification to reveal the effect of the matrices' intrinsic properties (such as its phonon energy) on the emission range and efficiency of the visible-to-UV UC. The fluoride matrices for visible-to-UV UC mainly include the $LiYF_4$ and the $Lu_7O_6F_9$, the silicates matrices include the $Y_2Si_2O_7$ and Y_2SiO_5, and the aluminates matrix. In this part, the electron energy level and properties of Pr^{3+} ion, and the Pr^{3+} doped fluoride, silicates and aluminates will be discussed in detail.

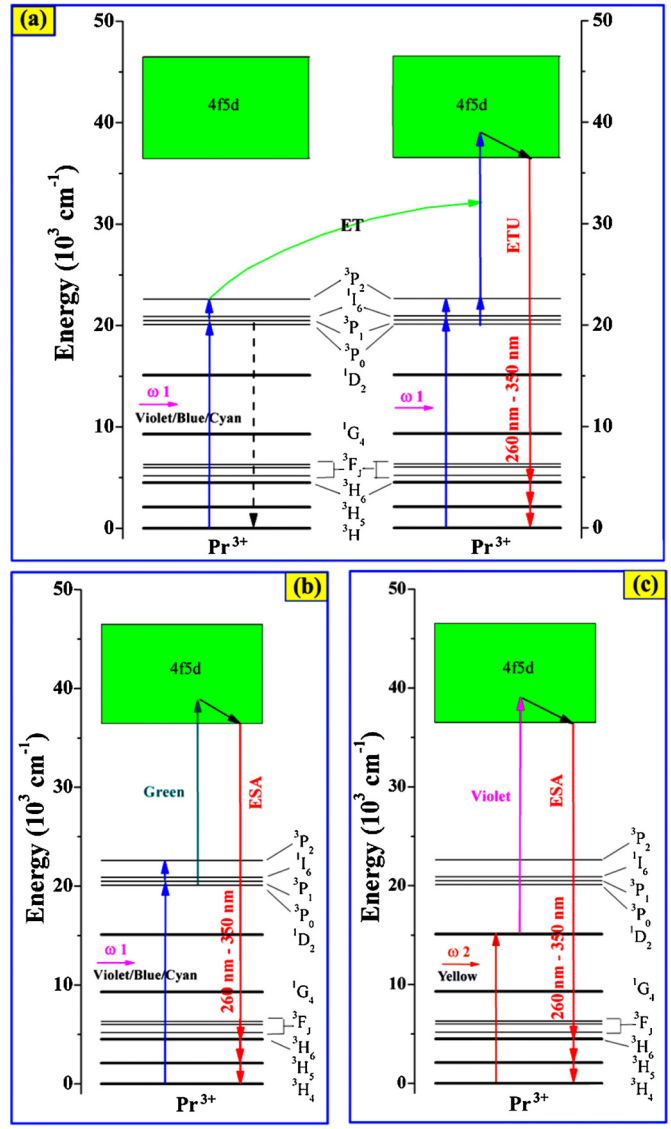

Fig. 4. ESA and ETU process of visible-to-UV UC excited by monochrome laser (A) and multi-colored laser (B, C) (Solid arrows depict light absorption or emission; dashed arrows depict energy transfer and non-radiative relaxation) [15].

3.1.1. The fluoride matrices

The $LiLuF_4$, and $LiYF_4$ and the $Lu_7O_6F_9$ were considered to be effective fluoride matrix for Visible-to-UV UC [21,23]. With the excitation of 488 nm laser or sunlight, UVC UC could be generated from the $LiYF_4$ microcrystal doped by Pr^{3+} ions ($LiYF_4$:Pr^{3+}). It is interesting to find that the excitation source variation resulted in different two-photon process for the visible-to-UV UC of $LiYF_4$:Pr^{3+}. When excited by 488 nm laser, the visible-to-UV UC of $LiYF_4$:Pr^{3+} is mainly attributed to the ETU process of excited Pr^{3+} ions. When excited by sunlight, not only the ETU process but the ESA the process contributed to the visible-to-UV UC of $LiYF_4$:Pr^{3+}, as the sunlight could be regarded as polychromatic and parallel light to facilitate the ESA process of different photons in the $LiYF_4$ matrix [23].

As shown in Fig. 6, the UVC UC of $Lu_7O_6F_9$:Pr^{3+} ceramics could be excited by 447 nm "blue-violet" continuous wave (CW) laser excitation (100 mW) [21]. In the $Lu_7O_6F_9$:Pr^{3+} ceramics, its lower phonon cutoff energy could decrease the $^3P_0/^1D_2$ multi-phonon relaxation rates and phonon-assisted $[^3P_0,^3H_4]/[^1D_2,^3H_6]$ cross-relaxation [21]. In addition, the low phonon energy of $Lu_7O_6F_9$ matrix is beneficial to prolong the lifetime of $Pr^{3+3}P_0$ level. Com-

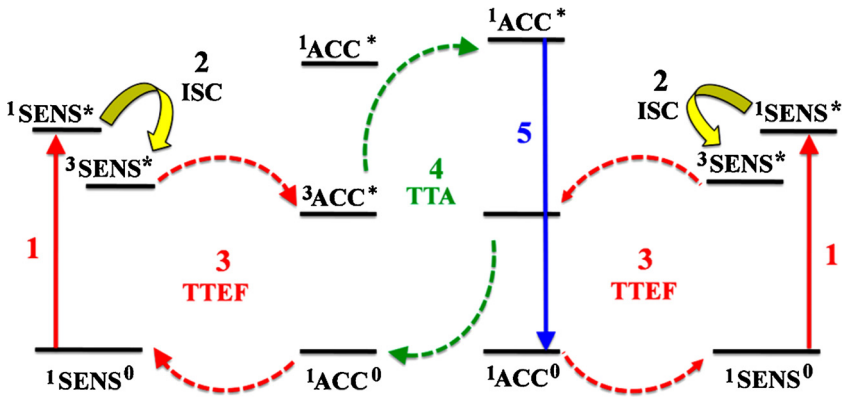

Fig. 5. The steps of TTA UC by organic: (1) low energy photon absorption by sensitizer, (2) singlet–triplet intersystem crossing of singlet, (3) triplet–triplet energy transfer from sensitizer to acceptor, (4) triplet–triplet annihilation, and (5) high energy photon emission. (SENS: sensitizer; ACC: acceptor; Dashed colored arrows: energy transfer by direct electron exchange; 1 and 3 respectively means the singlet and triplet state of organic molecules) [2,6].

pared with the 3.1 ms lifetime of Pr^{3+} P_0 level in Y_2SiO_5:Pr^{3+}, the $^3P_0$ lifetime of Pr^{3+} in $Lu_7O_6F_9$:Pr^{3+} could be prolonged up to 15.5 ms. Those intrinsic advantages make $Lu_7O_6F_9$ matrix to be the most efficient system to date to yield the visible-to-UV UC of Pr^{3+} ions.

3.1.2. The silicates matrices

In terms of the silicates matrices, the Y_2SiO_5 and β-$Y_2Si_2O_7$ matrix both exhibit potential to yield the visible-to-UV UC [9–11,13,15,18–20]. The Y_2SiO_5 is the matrix which was paid the most attention in the research field of visible-to-UV UC, while the β-$Y_2Si_2O_7$ matrix set a new record for the improvement of visible-to-UV UC. Herein, the structure and UC characteristics of the two matrixes are reviewed one by one in detail.

(1) The silicate matrix of Y_2SiO_5

■ The structure of Y_2SiO_5 matrix

The Y_2SiO_5 matrix is regarded to be an suitable candidate with high chemical and photochemical stability for the Ln^{3+} luminescent centers to emit Visible-to-UV UC [17,18,20,22,25,26]. The Y_2SiO_5 has two polymorphs phase [19]. The first phase has monoclinic unit cells with the space group of P21/c, and the Y^{3+} ions occupy two sites, that is, the 9-coordinated sites and 7-coordinated sites in its crystal. Fig. 7(a) illustrates the second phase of Y_2SiO_5 which also has monoclinic unit cells. Unlike the first phase, the second phase of Y_2SiO_5 has the space group of I2/a, and the Y^{3+} ions occupy 6-coordinated sites and 7-coordinated sites in its crystal.

■ ESA and ETU in Y_2SiO_5 matrix

In fact, the first phase of Y_2SiO_5 has little contribution to its Visible-to-UV UC, while the second phase provides a special coordinating environment for the Pr^{3+} to generate the visible-to-UV UC. When Pr^{3+} ions are doped into the second phase of Y_2SiO_5, the Pr^{3+} ions will replace the sites of some Y^{3+} ions in the matrix. The ETU and ESA energy transfer of Pr^{3+} ions will be generated when the matrix is excited by monochromic or polychromatic visible irradiations of violet, cyan, green, and yellow light, thus leading to the Visible-to-UV UC of Pr^{3+}:Y_2SiO_5 [22].

In the Y_2SiO_5 matrix, the ESA and ETU of Pr^{3+} both contribute to yield the visible-to-UV UC. The ratio of ETU to ESA process (ETU rate/ESA rate) depends on the concentration of Pr^{3+} ion, as the Pr^{3+} concentrations could also influence on the electron lifetime of Pr^{3+} $^3P_0$ level during the UC process [17,20]. Jiang et al. investigated in detail about that and calculated the UC ratio of ETU to ESA under the steady-state assumption. The UC ratio of ETU to ESA could be described as:

$$ETU\ \ rate/ESA\ \ rate = \frac{h\nu}{I\sigma_{23}}\left(1-\frac{\int_0^\infty I(t)dt}{I_0\tau_0}\right)R_2 \quad (1)$$

Where hν is the pump photon energy; I is the pump light intensity; σ_{23} is absorption cross-section from $^3P_0$ to 4f5d level; I(t) is the fluorescence intensity decay profile from the $^3P_0$ level, τ0 is the lifetime measured in the less concentrated crystal; R_2 is the decay rate of $^3P_0$ level.

According to Formula (1) and relative experiments, it was speculated that ETU process is the predominant UC mechanism when Pr^{3+} concentrations was high, while ESA is the predominant UC mechanism for lower Pr^{3+} concentrations [20].

■ Co-doping Li^+ and Gd^{3+} in Y_2SiO_5 matrix

In order to enhance the Visible-to-UV UC intensity, some researcher investigated modifying the crystal structure of the Y_2SiO_5 matrix and regulating the dispersion of Pr^{3+} ions in it by co-doping the Y_2SiO_5 matrix with Li^+ ions. The co-doping of Li^+ ions were proved to be effective to promote the Visible-to-UV UC, and the positive effect of Li^+ ions could mainly be attributed to three intrinsic reasons. Firstly, the $^3H_4 \rightarrow {}^3P_J$, $^1I_6$ transition probabilities were promoted due to the crystal asymmetry induced by Li^+ doping [15]. Secondly, the Li^+ ions in the silicates facilitate the Pr^{3+} clusters to spread and distribute more homogeneously in the matrix, due to the minimizing the detrimental cross relaxation (CR) between two excited neighboring Pr^{3+} ions [19]. Thirdly, the Li+ doping could induce the formation of much larger crystallites, in which the irradiation energy could be transfer with higher efficiency [21]. In addition, the Visible-to-UV UC could also be enlarged and promote the emission of 314 nm UC fluorescence by co-doping the Pr^{3+} ions with Gd^{3+} ions. As illustrated in Fig. 8, the effect of Gd^{3+} ions results from the energy transfer between the Pr^{3+} ions and the Gd^{3+} ions [15].

(2) The silicate matrix of β-$Y_2Si_2O_7$

■ The structure of β-$Y_2Si_2O_7$ matrix

The pyrosilicate β-$Y_2Si_2O_7$ is considered to be another highly potential candidate for the improvement of visible-to-UV UC quantum efficiency [16]. The pyrosilicate $Y_2Si_2O_7$ is a complex kind of material, which have seven different polymorphism structure including the α, β, γ, δ, y, ζ, and η phases [27]. Only the β phase of

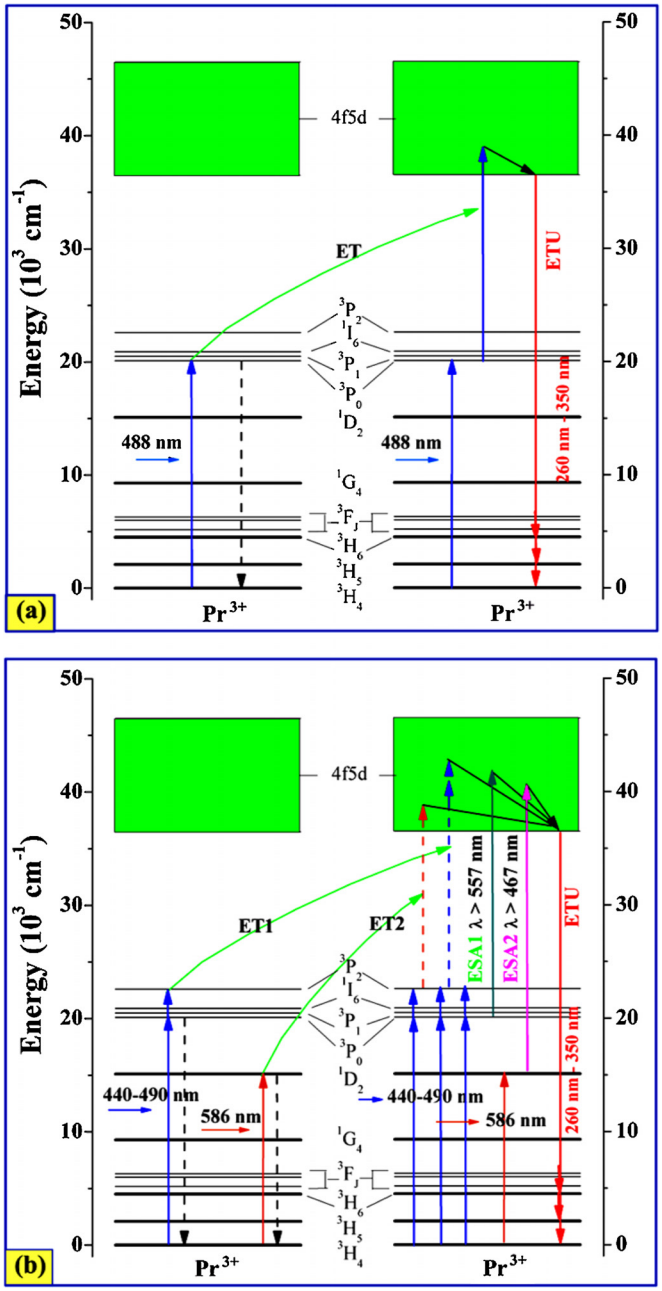

Fig. 6. Energy-level diagrams and absorption spectrum of the Pr^{3+} ion and energy transfer mechanisms in $Lu_7O_6F_9$:Pr^{3+} ceramics (a) under the 488 nm laser (b) under sunlight.

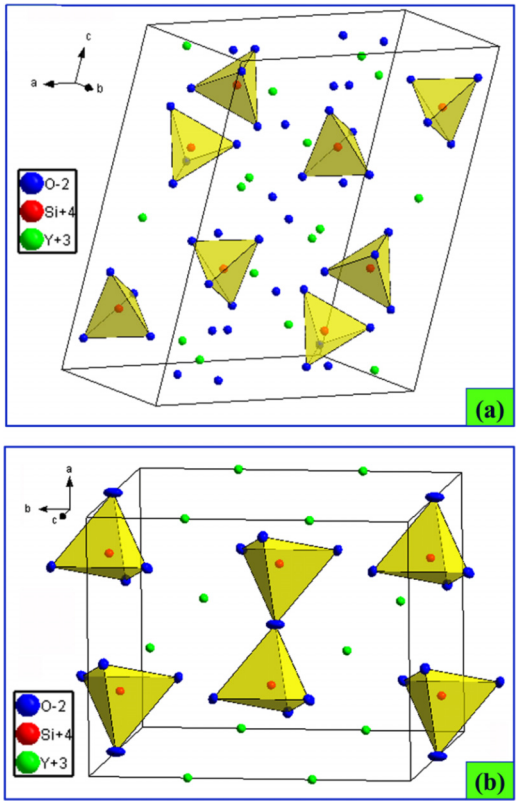

Fig. 7. Structure of (a) Y_2SiO_5 (space group I2/a), and (b) β-$Y_2Si_2O_7$ (blue = O^{2-}, red = Y^{3+}, yellow = $[SiO_4]^{4-}$ tetrahedral, green = Si^{4+}). (For interpretation of the references to colour in this figure legend, the reader is referred to the web version of this article.)

$Y_2Si_2O_7$ (β-$Y_2Si_2O_7$) was reported to possess the Visible-to-UV UC capability. Fig. 7(b) illustrates a unit cell structure of β-$Y_2Si_2O_7$, which crystallizes into a monoclinic structure with the C12/M1 space group, in which the Y^{3+} cations only occupy the distorted octahedral site. The structure of β-$Y_2Si_2O_7$ allows for a good solution of Ln^{3+} in its matrix without disturbing its structure.

■ Modified ETU model in β-$Y_2Si_2O_7$ matrix

Cates et al. found that the Pr^{3+} doped β-$Y_2Si_2O_7$ exhibited larger Visible-to-UV UC intensity and higher quantum efficiency than that of the Pr^{3+} doped Y_2SiO_5 [16]. It should be marked that the Pr^{3+}:β-$Y_2Si_2O_7$ they prepared could yield the most efficient Visible-to-UV UC to date. Compared with the Pr^{3+}:Y_2SiO_5, the β-$Y_2Si_2O_7$ matrix

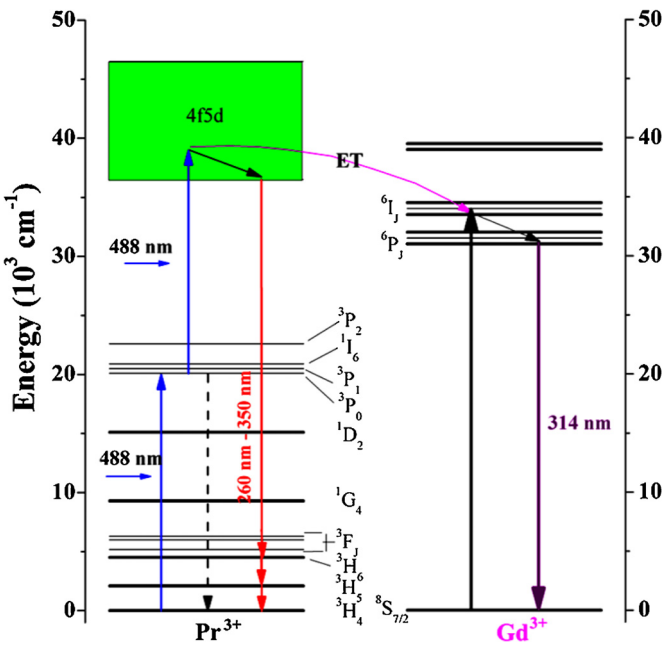

Fig. 8. Upconversion mechanisms of Pr^{3+} and Gd^{3+} UV emissions [21] (Solid blue line shows visible light absorption; dotted black line shows nonradiative energy transfer; dotted purple line shows UV photon emission). (For interpretation of the references to colour in this figure legend, the reader is referred to the web version of this article.)

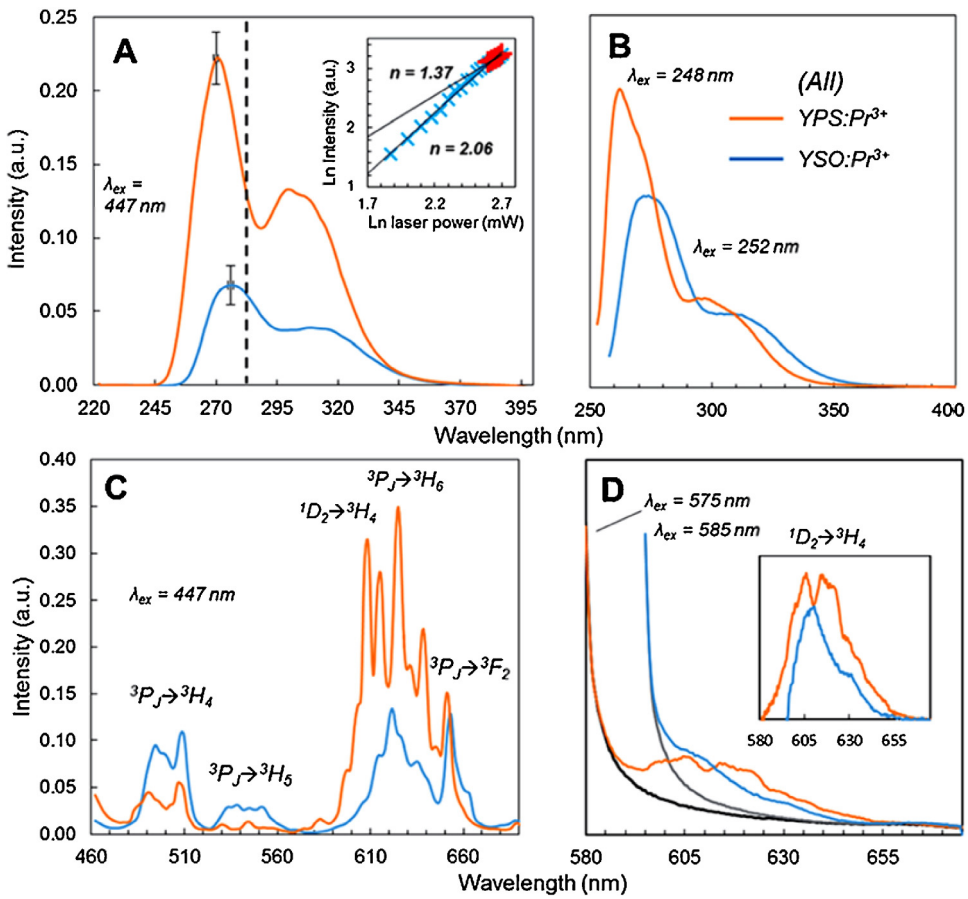

Fig. 9. Emission spectra of Pr^{3+}:β-$Y_2Si_2O_7$ (orange) and Pr^{3+}:Y_2SiO_5 (blue) ceramics [9] (A) UC emission under 447 nm excitation; dotted line shows upper boundary of UVC region; inset: the visible-to-UV UC of the Pr^{3+}:β-$Y_2Si_2O_7$ excited by irradiation with high and low power intensity; slopes [n]: linear regressions of double-logarithmic data; error bars: peak height standard deviation of three separately prepared samples. (B) Stokes emission by UVC excitation. (C) Stokes emission under $^3P_2$ (447 nm) excitation. (D) Modified ETU model for the visible-to-UV UC of the Pr^{3+}:β-$Y_2Si_2O_7$. (Cited from Ref. [9]). (For interpretation of the references to colour in this figure legend, the reader is referred to the web version of this article.)

resulted in a 3.1-fold increase in overall UC emission range and 3.9-fold increase in the germicidal range (l < 280 nm). Cates et al. ascribed the large improvement of Visible-to-UV UC to the modified ETU process of Pr^{3+} ions in the β-$Y_2Si_2O_7$ matrix [16]. In the modified ETU process, the $^3H_4 \rightarrow {}^3P_0$ transition co-existed with the fast $^3P_J \rightarrow {}^1D_2$ relaxation and the long-lived $^1D_2$ state. The lifetime of the $^1D_2$ state is 1–2 orders of magnitude than other intra-4f transitions due to its spin-forbidden nature. Owning to the long life of the $^1D_2$ state, the $^3P_J \rightarrow {}^1D_2$ relaxation is beneficial to excite stronger anti-Stokes emission to release higher Visible-to-UV UC.

Besides, the anti-Stokes Visible-to-UV UV emission of the Pr^{3+}:β-$Y_2Si_2O_7$ shifted toward higher energy and was sharper than that of the Pr^{3+}:Y_2SiO_5, as shown in Fig. 9(A) [9]. So does that of the Stokes emission, as shown in Fig. 9(A–C). The shift and sharpness of the Visible-to-UV UV emission is attributed to the structure characteristic of the β-$Y_2Si_2O_7$ crystal. As discussed above, in the β-$Y_2Si_2O_7$ lattices, the Pr^{3+} or Y^{3+} ions only occupy one crystallo-graphically site, that is, the distorted octahedral site. In the Y_2SiO_5 lattices, the Pr^{3+} or Y^{3+} ions occupy two different sites, a 6-coordinated site and a 7-coordinated site [16,27]. Thus, the Visible-to-UV UV emission of the Pr^{3+}:β-$Y_2Si_2O_7$ was sharper than that of the Pr^{3+}:Y_2SiO_5, as the UC fluorescence of Pr^{3+}:β-$Y_2Si_2O_7$ was released from single species of Pr^{3+} site whereas the UC fluorescence which released from two species of Pr^{3+} sites of Pr^{3+}:Y_2SiO_5 overlapped with each other.

3.2. Organic sensitizer/acceptor systems

In the organic sensitizer/acceptor system, it is necessary to select the acceptor and sensitizer for the generation of the visible-to-UV UC. According to the TTA mechanism mentioned above, the acceptor compound should has both a triplet state and a singlet state, while the excited state energy levels of the sensitizer should be sandwiched in-between those of the acceptor. Thus, it demands highly for the energy level matching between the organic acceptor and the sensitizer [6].

There are limited numbers of organic sensitizer and acceptor molecules whose energy level could be matched suitably to meet such high demands. The organic and metallo-organic compounds were usually applied as the triplet sensitizer and acceptor to yield visible-to-UV UC effectively [6]. The most effective sensitizers are metallo-organic complexes, namely the porphyrin derivatives coordinated to platinum group cations (e.g., Ru(II) polyimine complexes or Pt(II)/Pd(II) porphyrin complexes), as these compounds result in exceptionally long excited state lifetimes due to metal-to-ligand charge transfer.

4. Characteristic strategies for the visible-to-UV UC material

As discussed in Section 3, optical properties of Ln^{3+}-doped inorganic visible-to-UV UC materials not only depends on the electron

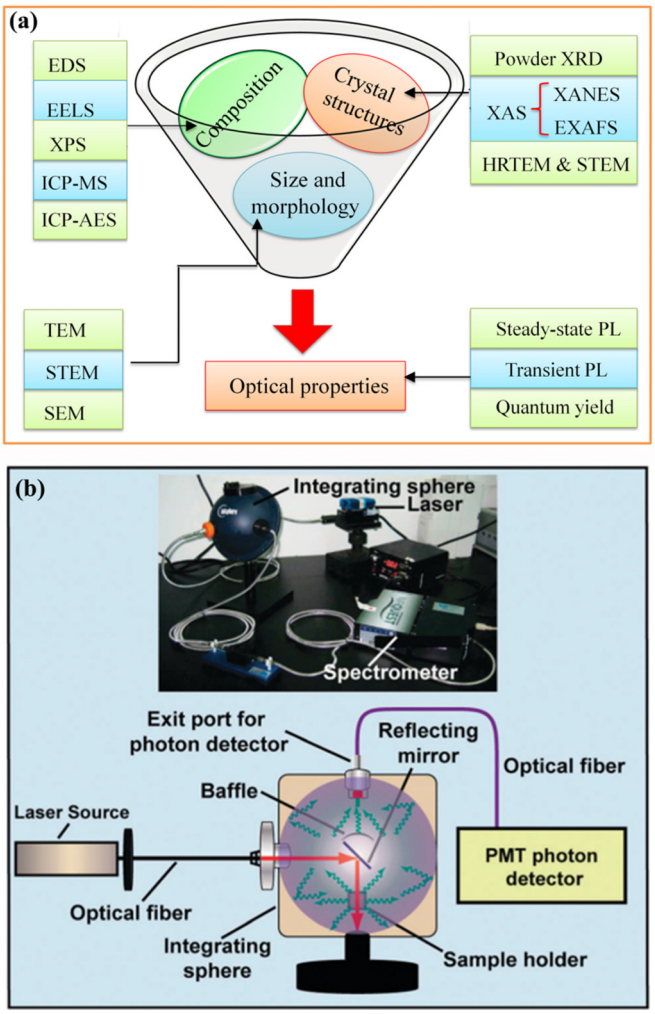

Fig. 10. (a) Characteristic strategies for the Visible-to-UV UC material (b) Scheme of the integrating sphere. (Cited from Ref. [1]).

level, concentration and distribution of the Ln^{3+} ions, but on the composition, crystal structure and energy transfer capability of the host matrix. In order to clarify intrinsic UC optical mechanisms for the UC materials, not only the existing state and distributions of Ln^{3+} ions but the nature of the host matrix should be characterized to provide enough evidence. In consequence, the characteristic strategies we discuss in this section mainly focus on the optical measurement, crystal structure analysis, size and morphology detection, as well as the composition and elements characterization, as illustrated in Fig. 10(a).

4.1. Optical characterization strategies

Photoluminescence (PL) characterization provide essential and direct evidence for investigating intrinsic energy transfer mechanism of the visible-to-UV anti-stokes UC emission. Optical characterization for visible-to-UV UC mainly includes steady-state PL measurements, transient PL measurements, and UC quantum yield detection.

(1) Steady-state PL measurements

As for steady-state PL measurements, it is essential to choose appropriate excitation source and excitation wavelength for UC detection. Due to low conversion efficiency and nonlinear optical nature of visible-to-UV UC, the energy of xenon lamp and tungsten lamp is too weak to excite strong enough UV irradiation for fluorescence measurement. As a result, continuous wave (CW) laser is required as excitation source to yield strong enough visible-to-UV UC for steady-state UC measurement. Single-line mode argon-ion laser and 100–1000 mW diode Pumped Solid State laser (DPSS) are both reported to be effective sufficient to trigger visible-to-UV UC for detecting [15,17].

(2) Transient PL measurements

In transient UC measurement for lifetime, a pulse laser is necessary to provide the time-dependent UC signal within two pulses, thus obtaining suitable time-resolved UC emission spectra by setting appropriate delay time and gate time within the temporal domain of Ln^{3+} luminescence [1]. In other word, pulse width of pulse laser excitation could be tuned comparable to the lifetimes of the intermediate states of Ln^{3+} activators (micro-second or millisecond) to enlarge the UC quantum yield [13]. During transient UC measurement, it is not suitable to reduce the pulse width to be shorter than the lifetime of the Ln^{3+} ions' intermediate state, otherwise the UC quantum yield would endure negligible impact. The lifetime measurement not only could help researchers to consider the intrinsic mechanism for Visible-to-UV UC, but provide direct structural information for the Visible-to-UV UC material as lifetime is closely related to the size and phase of material matrix as well as the doping concentration of Ln^{3+} activators.

(3) Absolute quantum yield measurements

Except for the steady-state and transient PL measurements, absolute quantum yield (Φ) of UC is also a significant optical parameter, which could evaluate the Visible-to-UV conversion efficiency. There are two important components for the measurement of the absolute quantum yield. One is an integrating sphere by which the emission from the UC materials are scattered and an extended spectrometer for analyzing the scattered photons, as illustrated in Fig. 10(b).

Herein, Φ could be calculated by Formula 2:

$$\phi = \frac{N_{emission}}{N_{absorption}} = \frac{L_{sample}}{E_{sample} - E_{sample}} \quad (2)$$

where $N_{emission}$ relates to the number of UC photons, and $N_{absorption}$ means the number of photons absorbed, L_{sample} means the integrated emission peaks, $E_{reference}$ and E_{sample} are the respective integrated excitation peak after absorption (or scattering) of the reference and specimen.

4.2. Crystal structure characterization

As discussed above, Visible-to-UV UC efficiency depends highly on the structure of material matrix. For example, only the β-$Y_2Si_2O_7$ was reported to possess the Visible-to-UV UC capability, though the pyrosilicate $Y_2Si_2O_7$ have seven different polymorphism structure including the α, β, γ, δ, y, ζ, and η phases [27]. Besides, in the fluoride matrixes, UC efficiency of hexagonal $NaYF_4$ could be ten times higher than that of its cubic counterpart. Consequently, it is important to investigate the crystal structure of UC materials, as they provide different chemical environment for the doped Ln^{3+} ions to result in enormous variation of UC efficiencies. In this section, two characterization techniques are summarized in detail for the structural characterization of UC materials, including the powder XRD and XAFS spectroscopy.

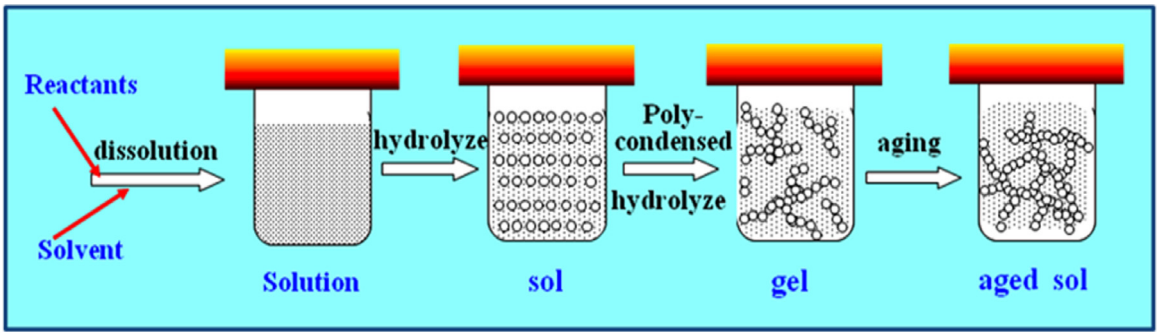

Fig. 11. The process of sol-gel technique for the synthesis of Visible-to-UV UC material.

4.2.1. Powder XRD

Based on Bragg's Law (Formula (3)), the Powder XRD is a conventional and effective method to identify the crystal structure of materials. Generally speaking, Powder XRD could provide at least three important crystal information for researchers to investigate the relationship of material matrixes to their special UC performance.

$$2d\sin\theta = n\lambda \tag{3}$$

(1) Crystal structure and phase transition information

Powder XRD could identify the crystal structure and phase transition of UC materials, thus make it convenient to investigate the effect of crystal variation. For example, it is interesting to find that inserting transition metal dopants into the fluoride matrix facilitate its phase transformation from hexagonal to cubic. Dou and Zhang reported that the doping of small-sized alkaline metal ions, such as Li^+, could also promote the hexagonal → cubic → tetragonal phase transformation of fluoride matrixes. Optical properties of UC materials therefore could be manipulated because the energy transfer pathways of Ln^{3+} ions varied with their local environment.

(2) Size information

Powder XRD also provides the crystal information about the average size of UC materials. Size information is also significant to evaluate the optical property of UC material, considering the energy transfer of Ln^{3+} ions is influenced by the of crystallization condition and surface situation of the UC material. For example, it was found that Ln^{3+} ions can not only promote the transformation from cubic phase to hexagonal phase but give rise to the formation of smaller nano-crystals in the fluoride matrix, thus endowed the fluoride material with tunable UC properties [28].

$$D = \frac{K\lambda}{\beta\cos\theta} \tag{4}$$

The size of nano UC materials could be evaluated by Scherrer's equation (formula 4). Herein, K is the crystallite-shape factor, λ is the wavelength of the incident X-ray, β is the corrected half width of the diffraction peak and θ is the diffraction angle. (Formula (3) works only when the material size is less than 100 nm).

(3) Stress information in material lattice

Powder XRD is capable of estimating the stress in crystallites, based on Williamson–Hall theorem (Formula (5)). Lattice stress, which includes the tensile and compressive strain, is also an important parameter to regulate the UC property due to its influence on the optical and electronic and photophysical properties of nano UC materials.

$$\frac{\beta\cos\theta}{\lambda} = \frac{1}{D} + \frac{\eta\sin\theta}{\lambda} \tag{5}$$

where K is the crystallite-shape factor, λ is the wavelength of the incident X-ray, β is the corrected half width of the diffraction peak and θ is the diffraction angle, D is the average particle size and η is the strain, respectively.

4.2.2. X-ray absorption spectrum (XAS)

XAS spectroscopy has great contribution to reveal local structures around the Ln^{3+} doped in the matrix of UC materials. XAS spectrum could be classified into two groups, including X-ray absorption near-edge spectroscopy (XANES) and extended X-ray absorption fine-structure spectroscopy (EXAFS). Both XANES and EXAFS are based on the X-ray photoelectric effect and the wave nature of the electrons.

The application of XANES an EXAFS provide remarkable useful structure information for researcher to study the influence of local environment of Ln^{3+} dopants on their UC emissions. On one hand, they are capable of investigating formal oxidation state, coordination geometry, and inter-atomic distances of the Ln^{3+} atoms in UC material matrix. On the other hand, both XANES an EXAFS have low detection limits (down to ppm), thus local coordinating environment of Ln^{3+} can be analyzed in detail even if the Ln^{3+} atoms have low concentration in the lattices. It has been found that the UC emission Ln^{3+} ions in the matrix could be enhanced by introducing Li^+ ions into the matrix to reduce the symmetric environment around the Ln^{3+} ions [1].

4.2.3. HRTEM and STEM

HRTEM offers valuable information for inspecting the crystallographic structure, the crystalline defects and crystallite domains of UC materials. Compared with Powder XRD, HRTEM can be carried out on a single crystal grain or particle to resolve nano-scaled phase transformation and structural environment around Ln^{3+} ions by images Fourier transform whereas the Powder XRD could only provide overall structure information for piles of particles [28].

Furthermore, when equipped with a focused electron probe, TEM can be operated in the scanning mode to perform point-by-point scanning across samples and generate impressive imaging resolution down to sub-Ångstrom under an accelerating voltage of 300 kV (STEM). Consequently, STEM show great potential in resolving each single atom in the Visible-to-UV UC materials, as well as revealing the structural information of core-shell UC materials.

4.3. Size and morphology characterization

Size and morphology have important influence on both the optical performance and practical application of UC materials. Reg-

ulating the size of UC materials could lead to the variation of their optical performance, as the crystallization, lattice stress and surface scattering conditions of them change with their size. Besides, nano-scaled UC material could exhibit novel and exciting optical properties due to their nano effect. As for the practical application, for instance, nano scaled UC materials are more suitable for bioimaging or biolabeling than their large-sized equivalents. As a result, characterizing the size and morphology of UC material is also crucial to reveal the intrinsic mechanism of their optical performance.

TEM, STEM and SEM are inevitably three key techniques to display the morphology and size of UC materials. Compared with optical imaging, the three electron microscopy techniques use electron beams to construct specimen images with higher resolution, better quality and more information. SEM is a convenient method for high resolution imaging by utilizing secondary electrons, or backscattered electrons or a mixture of them. SEM is easy to operate but could only detect the surface situation of UC materials (about 100 nm depth). In order to characterize UC materials with low conductivity, it is necessary to coat the material with a thin layer of Pt or carbon. As for TEM technique, it not only could provide the information of size and morphology, but are capable of exhibit the lattice mismatch and crystal growth mechanism of the UC material. Furthermore, TEM is especially useful to characterize core-shell UC materials and the formation of heterostructures in UC materials, owing to the diffraction contrast (brightness) differences in TEM imaging. As for STEM, its high-angle annular dark-field (HAADF) imaging mode is excellent for distinguishing the interfacial region of core–shell UC materials, as heavy atoms can yield high-angle scattered electrons to promote the contrast difference of HAADF-STEM imaging [28].

4.4. Composition and elements concentration characterization

As discussed above, UC optical property of Ln^{3+}-doped inorganic UC materials depends highly on the existing state, concentration and distribution of the Ln^{3+} ions. In consequence, it is necessary to explore effective instrumental techniques to reveal the situation of Ln^{3+} ions. Until now, there are mainly four microanalytical techniques to fulfill that purpose, including EDS, EELS, XPS, as well as ICP-MS and ICP-AES.

4.4.1. EDS, EELS and XPS characterization

EDS provide information of elemental composition by bombarding the UC materials with high energy electron beam. EDS could be applied together with TEM to obtain elemental mapping images for UC materials. Spatial resolution of EDS is approximately 1–10 nm. The line-scanning mode of EDS could effectively characterize the elements distribution of core-shell UC materials. Though detection limit of EDS can reach 0.1 at%, it is still a challenge to quantitatively analyze the concentration of doped Ln^{3+} ions in the material matrix due to the interference of impurities.

EELS technique is capable of providing the qualitative and quantitative analysis for dopants in UC materials by inspecting the energy loss of incident electron beam. Compared with EDS, EELS has better spatial resolution (0.1–1 nm), lower detection limit (0.05%), and faster characterization speed, whereas stronger background signals. The 1D or 2D scanning mode of EELS is especially suitable for analyzing the elements distribution of core-shell UC materials. Moreover, compared with EDS technique, EELS analysis bring less damage to the UC materials.

XPS is a useful probing technique with focused X-ray beam as light source to realize qualitative and quantitative analysis for surface composition. Compared with EDS and EELS, XPS has higher sensitivity (down to ppm), lower detection limit (0.01–0.5 atom%) and higher spatial resolution (5–30 mm), as shown in Table 2 [1].

Table 2
Comparison of EDS, EELS and XPS [1].

Technique	Incident source	Spatial resolution (nm)	Detection limit (atom%)
EDS	Electron beam	1–10	0.1
EELS	Electron beam	0.1–1	0.05
XPS	X-ray	5000–30 000	0.01–0.5

Though XPS measurement is limited to characterize material surface with a thickness of less than 10 nm, it can offer very useful information to clarify the concentration gradient of Ln3+ ions on UC materials surface.

4.4.2. ICP-MS and ICP-AES characterization

EDS, EELS and XPS all focus on the micro-domain analysis, while the ICP-MS and ICP-AES are applied to probing average concentrations of Ln^{3+} ions in the whole Ln3+ doped UC matrix. The detection limit of ICP-MS is about one order of magnitude higher than that of ICP-AES.

ICP-MS could detect Ln^{3+} ions with low concentrations by ionizing the sample with inductively coupled plasma and then using a mass spectrometer to separate and quantify those ions. The advantages of ICP-MS include its rapid speed, high precision, and sensitivity. The main limitation of ICP-MS measurement is that many interfering species are introduced into the detection system, such as argon from the plasma, component gases of air that leak through the cone orifices, and contamination from glassware and the cones. ICP-AES is an emission spectroscopy which utilizes inductively coupled plasma to produce excited atoms and ions that emit electromagnetic radiation at wavelengths characteristic of a particular element. It is a flame technique with a flame temperature in a range from 6000 to 10000 K. The concentration of the Ln^{3+} ions is revealed by the emission intensity.

5. Synthesis technique for the visible-to-UV UC material

In terms of the organic sensitizer/acceptor systems, it needs delicate design for the structure of sensitizer and acceptor, thus they could have suitable LUMO and HOMO energy level to realized effective energy level matching. In this section, it mainly discussed the synthesis technique of lanthanide-doped inorganic phosphors for Visible-to-UV UC [13].

5.1. Solid state reaction

The solid state reaction is a traditional but effective method for the synthesis of lanthanide-doped inorganic phosphors. Both the fluoride and the silicates matrix could be synthesized by the solid state reaction. During the solid state reaction, the reactants were melted and interact with each other to form new phase under calcination by high temperature. For the synthesis of Visible-to-UV UC material, the temperature is usually higher than 1000 °C to promote the reactants reacting at an appreciable rate.

The reaction rate of a solid state reaction depends not only on the structure, size, morphology, surface area and reactivity of the reactants, but on the calcinations temperature, the atmospheres and the thermodynamic free energy change associated with the reaction. In most cases, it is necessary to grind and mix the reactants before heating them, thus they could contact each other thoroughly and react more rapidly during the solid state reaction. Recently, some researchers facilitated the mixing process by blending the reactants via liquid co-precipitation. Some researchers promoted the solid state reaction rate and decreased the reaction temperature by use of nano scaled crystalline powder materials as reactants, as

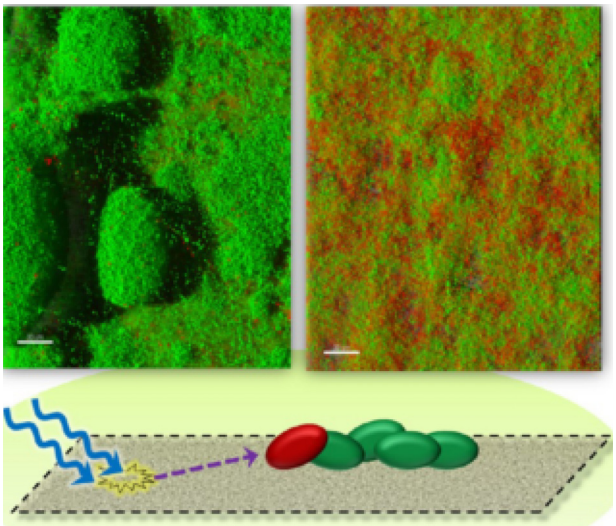

Fig. 12. (A) Confocal scanning laser microscope images of the cells growing on glass (left) and the glass decorated with Visible-to-UV UC material (Green represents cells with intact membranes, and red shows cells represents cells whose membranes were deteriorated). (Cited from Ref. [21]). (For interpretation of the references to colour in this figure legend, the reader is referred to the web version of this article.)

the nano materials have larger surface areas than bulk material and higher surface energy [19].

5.2. Sol-gel technique

The sol-gel technique is an effective wet-chemical technique for the fabrication of Visible-to-UV UC material of silicates matrix. In the sol-gel process, the monomers in the solution are hydrolyzed and poly-condensed to form a colloidal solution (the sol), and the sol then poly-condensed to form the network polymer structure of gel which contains both a liquid phase and a solid phase, as shown in Fig. 11. Further calcination is need to evaporated the liquid in the gel and promote the reaction for the atoms in the gel.

Compared with the mixture of reactants powders in solid state reaction, the atoms or molecules of the reactants are mixed more thoroughly in the gel to provide the sol-gel technique with two advantages over the solid state reaction. For one thing, the gel has lower calcinations temperature than reactants powders for the formation of new phase, because less energy are needed for promoting the reactants' atoms to go together. For the other thing, the sol-gel technique could help the doped Li^+ and Gd^{3+} ions disperse well in the silicates matrix. The Li^+, Gd^{3+} and Y^{3+} ions were mixed homogeneously into the gel during the sol-gel process, and then migrated into the lattice sites of the silicates matrix when the gel was heat-treated [15]. The special formation process makes those ions distributed homogeneously in the lattice of the lanthanide-doped inorganic phosphors.

5.3. Hydrothermal synthesis technique

In the hydrothermal synthesis process, the Visible-to-UV UC material was formed by the dissolution and re-crystallization of reactants in hot water or solvents. Compared with the solid state reaction and sol-gel techniques, the advantage of hydrothermal method is its ability to create crystalline phases which are not stable at the melting point. Thus, the application of hydrothermal synthesis technique could yield the generation of novel materials which could not be synthesized via the solid state reaction and sol-gel method Also, the method is simple but efficient for the growth of good-quality crystals while maintaining control over their composition.

Moreover, it is convenient to regulate the morphology, size and exposed crystal planes of target materials by tuning the hydrothermal conditions, taking into account that the kinetics and thermodynamics of crystal growth depends highly on those hydrothermal conditions such as the hydrothermal temperature, the hydrothermal pressure, the dielectric constant of the solvents, and the state of the reactants. Taking the preparation of Li^+,Pr^{3+}:Y_2SiO_5 micro-crystals for instance, the Y^{3+} and Pr^{3+} were provided with larger reaction surface by applying the mesoporous silica MCM-48 as the silica source, thus the hydrothermal reaction rate was accelerated to synthesis high-quality Visible-to-UV UC micro-crystals [24].

6. Challenges in visible-to-UV UC material research field

6.1. Challenges for lanthanide-doped inorganic phosphors

The visible-to-UV UC of lanthanide-doped inorganic phosphors is limited by two challenges. For one thing, it is difficult to excite the UVC UC emissions from the lanthanide-doped inorganic phosphors by sunlight irradiation. In most cases, the UC of lanthanide-doped inorganic phosphors were excited by a laser or xenon lamp which has high power. Compared with the laser and xenon lamp, the power density of sunlight (full spectrum) is much lower, thus the sunlight irradiation could only excite very weak Visible-to-UV UC for the lanthanide-doped inorganic phosphors. For another thing, Visible-to-UV UC material meet the challenge of low quantum efficiency. Conversion efficiency of the Visible-to-UV UC material is much lower than that of current advance IR-to-visible UC material. The conversion efficiency of IR-to-visible UC material could reach higher than 4%, whereas the conversion efficiency of Visible-to-UV UC is less than 0.1% [19]. Those two challenges limited the practical potential of Visible-to-UV UC material in large scale. In consequence, there is still a long way to go for lanthanide-doped inorganic phosphors concerning about how to make the material work under lower excitation power and how to improve the Visible-to-UV UC conversion efficiency.

6.2. Challenges for organic sensitizer/acceptor systems

Challenges for organic sensitizer/acceptor systems mainly include their chemical instability, toxicity and high production cost. On one hand, due to poor chemical stability of the organic sensitizer and acceptor, it is difficult to apply organic sensitizer/acceptor systems for practical application [6]. Some researches proposed that the chemical stability of such system could be improved by purging oxygen from the system in time [6]. However, that strategy is difficult for commercialization, as it not only adds the complexity for applying the organic system, but makes it difficult to incorporate the systems into other materials and devices. On the other hand, toxicity is another challenge which highly limited practical application of organic sensitizer/acceptor [2,6]. Additionally, organic sensitizer/acceptor systems have high production cost, for the custom-synthesized metalloorganic complexes are usually explored as the sensitized/acceptor TTA pairs, whose high cost make the system difficult to be commercialized [2,6].

7. Perspective and potential applications of the visible-to-UV UC material

7.1. Perspective of lanthanide-doped inorganic phosphors

7.1.1. Potential in the biomaterial fields

Current research situations indicate high potential of Visible-to-UV UC phosphors in biomaterial application fields. The application

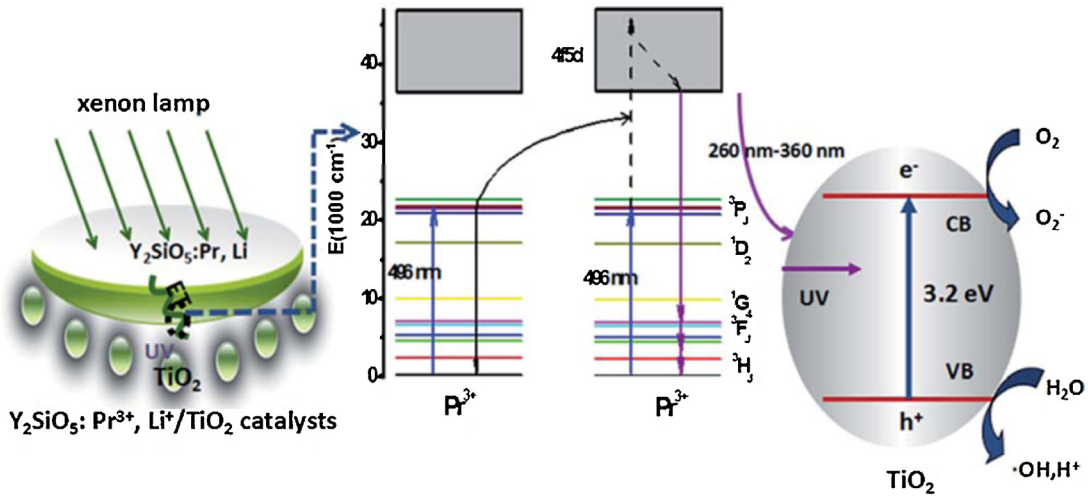

Fig. 13. Photocatalysis mechanism of Li^+,Pr^{3+}:Y_2SiO_5/TiO_2 catalyst (ET: energy transfer) (Cited from Ref. [17]).

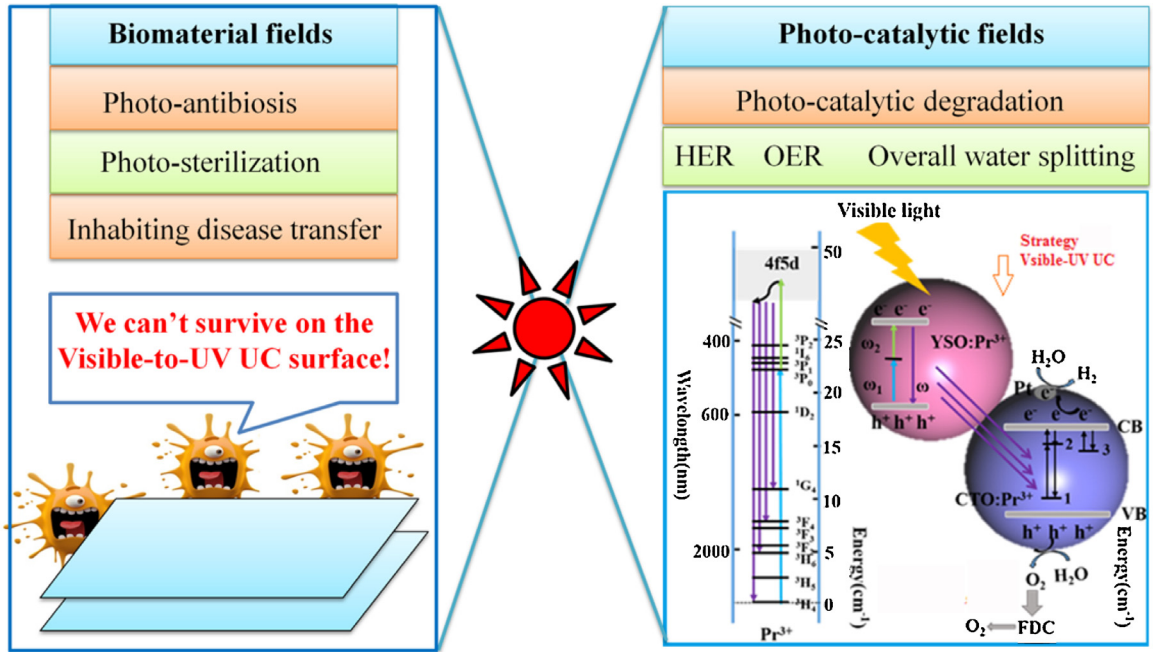

Fig. 14. Achievements and potential of visible-to-UV UC material in Biomaterial fields and Photo-catalytic fields (The blue ball means TiO_2 or Ti based UV-responsive photocatalysts, and the pink ball means the visible-to-UV UC material). (For interpretation of the references to colour in this figure legend, the reader is referred to the web version of this article.)

of Visible-to-UV UC materials as antimicrobial surface was first reported by Cates et al. in 2011, and they found the Visible-to-UV UC phosphors could still exhibit favorable performance in photo-antibiosis which are triggered by UV irradiations even though their Visible-to-UV UC conversion efficiency is lower than 0.1% [6]. As shown in Fig. 12, assembling the surface with Visible-to-UV UC material could effectively prohibit the growing of cell as the UVC inactivating and deteriorating their membranes. It could be expected that the Visible-to-UC UC materials could open a new window for promoting visible-light-driven photo-antibiosis and photo-sterilization to prevent disease transfer in hospitals, the food industry, and public areas in the future. Furthermore, Visible-to-UV UC antimicrobial material exhibited great commercial potential due to their convenience, low toxicity and high chemical stability, and low production cost [15].

7.1.2. Potential in photocatalysis

Taken more than 50% of the solar spectrum is in the range of visible region, the main obstacle in photocatalysis is development of stable, high efficient and low cost catalyst for hydrogen generation and toxic chemical elimination [28–59]. TiO_2 and Ti based photocatalysts are very active catalysts, but mainly respond to UV irradiation, so they could not make full use of the whole solar spectrum. Sulfide and Selenide based photocatalysts could work under visible light irradiation, but their practical applications are highly restricted due to their poor photo-chemical stability (photocorrosion). It could be expected that the visible-to-UV UC material will show remarkable potential in photocatalysis driven by solar energy by taking advantage of stable semiconductor photocatalysts sensitive to UV light. For instance, current research of visible-light-driven water splitting is highly limited due to absence of

efficient and chemically stable photo-catalysts. The application of visible-to-UV UC material can effectively sensitize UV-responsive photocatalysts to promote visible-light driven water splitting. Current research situations also indicate the Visible-to-UV UC materials have huge theoretical and commercial potential in these fields. Take Pr^{3+}:Y_2SiO_5 for an example, Yang et al. found that the Pr^{3+}:Y_2SiO_5 itself had photo-catalytic activity for the degradation of nitrobenzene due to its Visible-to-UV UC property [25]. When assembling it with UV-responsive photo-catalysts TiO_2, photo-catalytic degradation of MB dye could be accelerated up to 14 times by the Pr^{3+}:Y_2SiO_5/TiO_2 composite photo-catalys, indicating amazing capability of Visible-to-UV UC materials in photo-catalytic fields [24]. The acceleration of photo-catalytic degradation could be attributed to the UVB- and UVC-range photons generated by the ETU process of Li^+,Pr^{3+}:Y_2SiO_5, as shown in Fig. 13. Besides, $LiYF_4$:Pr^{3+} also show potential in photo-catalytic reactions triggered by solar energy, for they could release Visible-to-UV UC under sunlight excitation recently [23]. Though the $LiYF_4$:Pr^{3+} material released very low UVC which could only be captured by UV images under 63 mW/cm^2 sunlight irradiation, the research reported by Yang et al. indicate that its Visible-to-UV UC intensity can be regulated to improve in large scale by lowering the phonon energy of $LiYF_4$ matrix.

Those investigations suggest the enlightened future of the Visible-to-UV UC inorganic phosphors in photo-catalytic fields by taking full advantages of the special Visible-to-ultraviolet energy transfer process, not only from theoretical but from commercial perspective. In order to make full use of solar energy, current photo-catalytic researches pay much attention on visible-light-driven t photo-catalytic reactions, such as HER, OER and overall splitting water. Many efforts have been done to widen the responsive region of UV-responsive photo-catalysts. Those efforts mainly focus on matching the energy level of different photo-catalysts to regulate their band gap, which demand highly on the energy level matching degree of different photo-catalysts. Such limitation could be eliminated by the application of Visible-to-ultraviolet UC materials, as there is no need to consider the energy level matching of different photo-catalysts while all one need to do is just assembling a UV-responsive photo-catalysts with a Visible-to-ultraviolet UC unit. Consequently, it could be expected that the Visible-to-ultraviolet UC materials will play important theoretical and commercial role in photo-catalytic research fields by assembling them with UV-responsive photo-catalysts. The strategy is not only convenient and effective, but has favorable versatility for most UV-responsive photo-catalysts to realize overall split water by visible light irradiation.

7.2. Perspective of organic sensitizer/acceptor systems

Compared with lanthanide-doped inorganic phosphors, organic sensitizer/acceptor UC systems have two special merits including its higher UC quantum efficiency (external yields over 1%) and lower power required to excite Visible-to-UV UC (Table 1). As a result, organic sensitizer/acceptor UC systems also possess great potential for practical application despite of its low chemical stability and high toxicity and production cost [2]. Based on current research situation, the development of organic sensitizer/acceptor UC systems will focus on two aspects: (1) exploring more flexible and chemical stable molecular rationales to facilitate robust photo-physical properties; (2) assembling the organic sensitizer/acceptor UC systems with heterogeneous chemical stable material to construct composite material with robust Visible-to-UV UC, low toxicity and low production cost.

In conclusion, current research situations show notable advances and challenges of the visible-to-UV UC materials in theoretical research and practical applications. Fig. 14 summarized the achievements and potential of visible-to-UV UC materials based on recent progresses in that research field. Owning to its ability to manipulate and convert light energy, the visible-to-UV UC materials possess huge potential in anti-transfer of disease in hospitals, the food industry, and public areas in the future to benefit the public health issue of the world. Besides, they show amazing potential in photocatalytic fields to facilitate effective visible-light-driven photo-reactions like HER, OER and overall splitting water when combing them with high efficient UV-responsive photo-catalysts, thus beneficial for resolving the worldwide energy crisis and accompanied environmental problems. Moreover, the theoretical and commercial potential of visible-to-UV UC materials may be extended further to other relative optical research fields.

Notes

The authors declare no competing financial interest.

Acknowledgments

This work is supported by the NSF of China (21433007, 21673262), Natural Science Foundation of Jiangsu Province (BK20130095), and Postdoctoral Science Foundation of China (146819), respectively.

References

[1] X.W. Liu, R.R. Deng, Y.H. Zhang, Y. Wang, H.J. Chang, L. Huang, X.G. Liu, Chem. Soc. Rev. 44 (2015) 1479–1508.
[2] W. Wu, H. Guo, W. Wu, S. Ji, J. Zhao, J. Org. Chem. 76 (2011) 7056–7064.
[3] X. Huang, S. Han, W. Huang, X. Liu, Chem. Soc. Rev. 42 (2013) 173–201.
[4] H. Dong, L. Sun, C. Yan, Chem. Soc. Rev. 44 (2015) 1608–1634.
[5] X. Chen, D. Peng, Q. Ju, F. Wang, Chem. Soc. Rev. 44 (2015) 1318–1330.
[6] E.L. Cates, S.L. Chinnapongse, J.H. Kim, Environ. Sci. Technol. 46 (2012) 12316–12328.
[7] W. Feng, C. Han, F. Li, Adv. Mater. 25 (2013) 5287–5303.
[8] J. Liu, X.M. Tian, H.P. Chen, Y.Z. Shao, G.W. Yang, D.H. Chen, Appl. Surf. Sci. 348 (2015) 60–65.
[9] S.Q. Huang, Z.Y. Lou, Z.B. Qi, N.W. Zhu, H.P. Yuan, Appl. Catal. B: Environ. 168–169 (2015) 313–321.
[10] C.Y. Wang, X.H. Cheng, Appl. Surf. Sci. 371 (2016) 391–398.
[11] M.Y. Ding, S.L. Yin, D.Q. Chen, J.S. Zhong, Y.R. Ni, C.H. Lu, Z.Z. Xu, Z.G. Jia, Appl. Surf. Sci. 333 (2015) 23–33.
[12] T. Ikehata, Y. Onodera, T. Nunokawa, T. Hirano, S. Ogura, T. Kamachi, O. Odawara, Hiroyuki Wada, Appl. Surf. Sci. 348 (2015) 54–59.
[13] W. Zheng, P. Huang, D. Tu, E. Ma, H. Zhu, X. Chen, Chem. Soc. Rev. 44 (2015) 1379–1415.
[14] H.Y. Peng, B.B. Ding, Y.C. Ma, S.Q. Sun, W. Tao, Y.C. Guo, H.C. Guo, X.Z. Yang, H.S. Qian, Appl. Surf. Sci. 357 (2015) 2408–2414.
[15] E.L. Cates, M. Cho, J. Kim, Environ. Sci. Technol. 45 (2011) 3680–3686.
[16] E.L. Cates, F. Li, RSC Adv. 6 (2016) 22791–22796.
[17] C. Hu, C. Sun, J. Li, Z. Li, H. Zhang, Z. Jiang, Chem. Phys. 325 (2006) 563–566.
[18] Y. Yang, C. Liu, P. Mao, L. Wang, J. Nanomater. 2013 (2013) 1–7.
[19] W. Zheng, P. Huang, D. Tu, E. Ma, H. Zhu, X. Chen, Chem. Soc. Rev. 44 (2015) 1379–1415.
[20] C. Sun, J. Li, C. Hu, H. Jiang, Z. Jiang, Eur. Phys. J. D. 39 (2006) 303–306.
[21] E.L. Cates, A.P. Wilkinson, J.H. Kim, J. Lumin. 160 (2015) 202–209.
[22] E.L. Cates, J.H. Kim, Opt. Mater. (Amst.) 35 (2013) 2347–2351.
[23] J. Wu, H. Zheng, X. Liu, B. Han, J. Wei, Y. Yang, Opt. Lett. 41 (2016) 792–795.
[24] J. Wu, Y. Yang, Z. Wei, B. Han, J. Wei, RSC Adv. 4 (2015) 1166–1169.
[25] Y. Yang, G. Xia, C. Liu, J. Zhang, L. Wang, J. Chem. (2015) 938073.
[26] V.V. Seminko, A.A. Masalov, Y.I. Boyko, Y.V. Malyukin, J. Phys. Chem. C 116 (2012) 12772–12778.
[27] J. Sokolnicki, Mater. Chem. Phys. 131 (2011) 306–312.
[28] S. Zeng, J. Xiao, Q. Yang, J. Hao, J. Mater. Chem. 22 (2012) 9870–9874.
[29] Z. Li, B. Tian, W.Y. Zhang, X.Q. Zhang, Y.Q. Wu, G.X. Lu, Appl. Catal. B 204 (2017) 33–42.
[30] L. Ma, X. Kang, S. Hu, F. Wang, J. Mol. Catal. (China) 29 (2015) 359–368.
[31] C. Wu, Y. Fang, P. Zhao, J. Yang, M. Jia, Y. Huang, J. Mol. Catal. (China) 29 (2015) 369–381.
[32] Z. Li, B. Tian, W.L. Zhen, Y.Q. Wu, G.X. Lu, Appl. Catal. B 203 (2017) 408–415.
[33] B. Tian, W.L. Zhen, H.B. Gao, X.Q. Zhang, Z. Li, G.X. Lu, Appl. Catal. B 203 (2017) 789–797.
[34] C. Li, Z. Lei, Q. Wang, F. Cao, F. Wang, W.F. Shangguan, J. Mol. Catal. (China) 29 (2015) 382–389.
[35] L. Zhang, Y. Deng, F. Shi, J. Mol. Catal. (China) 29 (2015) 179–187.

[36] W.Y. Zhang, J. Chen, W. Wang, G.X. Lu, L. Hao, Y. Ni, C. Lu, Z. Xu, J. Magnet. Magnet. Mater. 426 (2017) 1–10.
[37] X.Q. Zhang, G.X. Lu, Carbon 108 (2016) 215–224.
[38] S. Sun, C. Li, W. Yang, X. Yan, Y. Zheng, L. Wang, J. Bian, J. Mol. Catal. (China) 29 (2015) 188–196.
[39] X. Wang, S. bai, Z. Bao, J. Mol. Catal. (China) 29 (2015) 266–274.
[40] W.L. Zhen, J.T. Ma, G.X. Lu, Appl. Catal. B 190 (2016) 12–25.
[41] Z. Li, Y.Q. Wu, G.X. Lu, Appl. Catal. B 188 (2016) 56–64.
[42] L. Li, Y. Huang, A. Zhang, M. Xiang, J. Yang, M. Jiao, J. Mol. Catal. (China) 30 (2016) 470–479.
[43] Z. Shen, J. Zhong, L. Wang, Y. Zhang, Y. Cui, L. Chen, J. Mol. Catal. (China) 30 (2016) 260–268.
[44] Y.P. Guo, G.X. Lu, Int. J. Hydrogen Energy 41 (2016) 6706–6712.
[45] Z. Li, C. Kong, G.X. Lu, Int. J. Hydrogen Energy 40 (2015) 9061–9068.
[46] P. He, Y. Chen, W. Fu, J. Mol. Catal. (China) 30 (2016) 269–275.
[47] G. Lu, S. Zhang, G. Hou, F. Shi, T. Li, X. Yao, H. Liang, J. Mol. Catal. (China) 30 (2016) 383–390.
[48] W.Y. Zhang, G.X. Lu, Catal. Sci. Technol. 6 (2016) 7693–7697.
[49] W.Y. Zhang, C. Kong, W. Gao, G.X. Lu, Chem. Commun. 52 (2016) 3038–3041.
[50] W.Y. Zhang, C. Kong, G.X. Lu, Chem. Commun. 51 (2015) 10158–10161.
[51] G. Lu, S. Zhang, Z. Lun, J. Zhang, Z. Hao, J. Lin, F. Wang, H. Liang, J. Mol. Catal. (China) 30 (2016) 383–390.
[52] C. Kong, Z. Li, G.X. Lu, Int. J. Hydrogen Energy 40 (2015) 5824–5830.
[53] E.T. Cui, G.X. Lu, Int. J. Hydrogen Energy 39 (2014) 7672–7685.
[54] Z. Li, Q.S. Wang, C. Kong, Y.Q. Wu, Kong, Y.Q. Wu, Y.X. Li, G.X. Lu, J. Phys. Chem. C 119 (2015) 13561–13568.
[55] G.X. Lu, S.B. Li, Int. J. Hydrogen Energy 17 (1992) 767–770.
[56] Y.X. Li, D. Gao, S.Q. Peng, G.X. Lu, S.B. Li, Int. J. Hydrogen Energy 36 (2011) 4291–4297.
[57] C. Kong, S.X. Min, G.X. Lu, Int. J. Hydrogen Energy 39 (2014) 436–4844.
[58] S.X. Min, G.X. Lu, Int. J. Hydrogen Energy 38 (2013) 2106–2116.
[59] S.X. Min, G.X. Lu, Int. J. Hydrogen Energy 37 (2012) 10564–10574.